Journal of Neuroscience Methods 215 (2013) 71–77

Contents lists available at SciVerse ScienceDirect

Journal of Neuroscience Methods

journal homepage: www.elsevier.com/locate/jneumeth

Computational Neuroscience

Gaussian Mixture Model-based noise reduction in resting state fMRI data

Gaurav Garg*, Girijesh Prasad, Damien Coyle

MS125, Intelligent Systems Research Centre, School of Computing and Intelligent Systems, Magee Campus, University of Ulster, Londonderry BT48 7JL, UK

HIGHLIGHTS

- The paper is about a noise reduction method for resting state fMRI data.
- Gaussian Mixture Model is used for classification of fMRI data.
- White and Rician noises were considered to test the efficiency of algorithm.
- The reference template for artificial data was completely noiseless.
- Given fMRI data was referenced as template to test for additional noise.

ARTICLE INFO

Article history:
Received 25 October 2012
Received in revised form 20 February 2013
Accepted 22 February 2013

Keywords:
Gaussian Mixture Model
Clustering
Noise
fMRI

ABSTRACT

Neuroimaging the default mode network (DMN) in resting state has been of significant interest for investigating pathological conditions as resting state data are less affected by the variability in the subject's performance and movement-related artefacts in the electromagnetic field which are often issues in event-related activation experiments. An issue to be considered with resting state data is the very low amplitude of the activation patterns which are not induced by any stimulation or stimulus paradigm. Though, many studies have suggested that amplitude of low frequency fluctuation (ALFF) analysis is suitable for resting state functional magnetic resonance imaging (fMRI) data analysis, the low signal-to-noise-ratio (SNR) of acquired neuroimaging data poses a significant problem in the accurate analysis of the same. In this work, a Gaussian Mixture Model (GMM) method to suppress the noise during data pre-processing before ALFF is applied (GMM-ALFF) is proposed, where the optimum numbers of Gaussian distributions are fitted to the data using the Bayesian information criterion (BIC). The method has been tested with artificial data as well as real resting state fMRI data collected from Alzheimer's disease patients with different levels of added noise. Improvement of as much as 40% for artificial datasets and at least 3% for real datasets ($p < 0.05$) have been observed when applying the proposed GMM approach prior to the analysis with the existing ALFF approach.

1. Introduction

Analysis of resting state neuroimaging data, while comparing the pathological conditions in disease against age matched healthy control subjects, has found displacement in the region of origin and decreased strength in the fMRI signal (Buxton et al., 2005; Raichle et al., 2001). Decrease in the signal strength has been defined by many as deactivation while an increase in the activity is considered as compensating behaviour of brain functions (Raichle et al., 2001). However, suppressions of activation cannot always be considered as 'deactivation' as some areas, which show this decrease in activity, are found to generate a significant level of activity during the rest state (Raichle et al., 2001). These activations have been found to show significant but slow (<0.08 Hz) rhythmic blood oxygen level dependent (BOLD) metabolic activity when recorded using Positron Emission Tomography (PET) and fMRI based neuroimaging techniques (Buxton et al., 2005).

Many studies have suggested the existence of a specific correlation pattern in such resting state Default Mode Networks (Raichle et al., 2001; Keller et al., 2011). Most commonly, the techniques included calculating correlation between signals obtained from various distant brain areas to develop some inference about the synchronization and connectivity pattern among them. Other methods using higher order statistics such as Independent Component Analysis (ICA), when applied on the resting state fMRI data, have also shown to be promising for detecting connectivity patterns in DMNs (Raichle et al., 2001).

Amplitude of Low Frequency Fluctuation (ALFF) is a method proposed to measure the temporal similarity of voxels within a given cluster in a voxel-wise fashion for the given range of frequency response (Yang et al., 2007). It was found that the brain areas with

* Corresponding author. Tel.: +44 28 71675085.
E-mail addresses: garg-g@email.ulster.ac.uk, gauravgarg4@gmail.com (G. Garg), g.prasad@ulster.ac.uk (G. Prasad), dh.coyle@ulster.ac.uk (D. Coyle).

0165-0270/$ – see front matter © 2013 Elsevier B.V. All rights reserved.
http://dx.doi.org/10.1016/j.jneumeth.2013.02.015

the highest ALFF were located within the default mode network (Raichle et al., 2001; Keller et al., 2011).The reliability of many of the proposed methods is an on-going issue because of a multitude of noise sources in the fMRI scanning environment. This noise can be of a non-biological as well as biological nature. Biological noise can be caused by human factors such as random neural processes and background brain activity not related to subject of interest, heart beats, breath cycle and anything causing physical movements, etc. Biological noise is generally reduced by training the subject and providing some aid to reduce head movement inside the scanning environment. Non-biological sources of noise are the gradual or abrupt change in fMRI magnetic fields due to thermal effect and drift in the fMRI magnets with time. Such types of noise reduce the SNR of sophisticated brain signals being recorded by fMRI devices and hence need to be better analysed by complex computational methods (Chen and Tyler, 2008). Here, we propose an improved method which is based on Gaussian Mixture Models (GMM) and shows greater robustness for noise compared to traditional ALFF. Our previous work has demonstrated successful application of a similar GMM (Garg et al., 2009, 2011a, 2011b) based method for fMRI data obtained during an auditory stimulus driven paradigm.

We have applied the proposed GMM-ALFF method to investigate the resting state DMNs on two types of data: (1) an artificially simulated data-set with additive white Gaussian noise (AWGN) and Rician noise (RN) (Sled et al., 1998) and (2) real fMRI data from six Alzheimer's disease (AD) patients provided in the Alzheimer's Disease Neuroimaging Initiative (ADNI) online data repository (Weiner et al., 2012). In the current work, we demonstrate the efficacy of combining the GMM approach with the ALFF through a comparative evaluation.

2. BOLD signals modelled by GMM

The BOLD signals (Buxton et al., 2005) of a human brain represented by voxels in an fMRI image can be assumed to be the result of interaction of a large number of neuronal activations in the brain. Therefore, an fMRI voxel value can be represented as a weighted sum of the individual effect of each of these activations. According to the central limit theorem, the weighted sum of a large number of independent random variables follows a Gaussian distribution (Garg et al., 2009, 2011a, 2011b). Moreover, for a better characterization of the neuronal activities in different brain regions, these BOLD fMRI signals can be considered a result of contributions from different sets of neuronal assemblies. A GMM is a weighted sum of a number of Gaussian distributed components (clusters). As GMMs comprise of multiple Gaussian components, these can realistically model fMRI images.

Assuming that an fMRI image is modelled by an N component GMM, with Gaussian mixture variable $x = (x_1, x_2, x_3, \ldots, x_N)$ generated from N stochastic processes, where a stochastic process n has a probability density function (PDF) $g_n(x/\theta_n)$, then the PDF for the mixture model will be:

$$g(\mathbf{x}|\Theta) = \sum_{n=1}^{N} \left(p_n g_n \left(\frac{x}{\theta_n} \right) \right), \tag{1}$$

where $g_n(x/\theta_n) = ((1/\sqrt{2\pi\sigma_n^2}) \exp(-(x-\mu_n)^2/2\sigma_n^2))$ and p_n is the proportion of the nth process in the given mixture, such that $p_n \geq 0$ and $\sum_{n=1}^{N} p_n = 1$, and $\Theta = \bigcup_{n=1}^{N} \theta_n$ is the set of parameters consisting of μ_n and σ_n.

The likelihood function for the given mixture model can be defined as:

$$l(\mathbf{x}|\Theta) = \prod_{j=1}^{K} \sum_{n=1}^{N} \left(p_n g_n \left(\frac{x_j}{\theta_n} \right) \right) \tag{2}$$

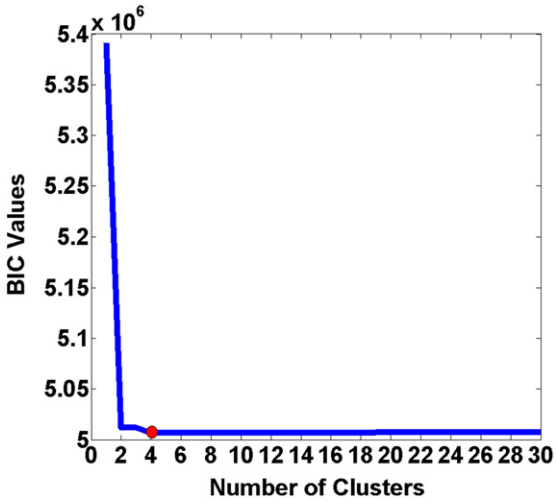

Fig. 1. BIC convergence plot for subject 1 with Rician Noise case, a red mark at 4th cluster shows the achieved minimum BIC value.

Here, K is the total number of observed data samples and x_j is the jth observation. We take the logarithm of the likelihood function to make it easier to calculate.

$$L(\mathbf{x}|\Theta) = \sum_{j=1}^{K} \left(\ln \sum_{n=1}^{N} \left(p_n g_n \left(\frac{x_j}{\theta_n} \right) \right) \right) \tag{3}$$

So the complete log-likelihood function for GMM can be given as

$$L(\mathbf{x}|\Theta) = \sum_{j=1}^{K} \left(\ln \left(\sum_{n=1}^{N} p_n \left(\frac{1}{\sqrt{2\pi\sigma_n^2}} \exp \left(-\frac{(x_j-\mu_n)^2}{2\sigma_n^2} \right) \right) \right) \right) \tag{4}$$

The Bayesian Information Criterion (BIC) is then applied to select the optimal number of clusters as it was suggested as best among other available criteria including log likelihood, Akaike's information criterion (AIC) and Weighted AIC for biological data of coronary heart disease (Fonseca, 2008), BOLD fMRI data (Garg et al., 2011a) and statistical data for patient care management (Garg et al., 2009, 2011b). BIC is estimated as follows:

$$BIC = 2L(\mathbf{x}|\Theta) + C \ln(K) \tag{5}$$

Here, K is the total number of observed data samples and C is the degrees of freedom for the number of free parameters. Each of the distributed mixture has three characteristic parameters, sample mean, standard deviation and proportion of contribution of that cluster. So the degrees of freedom for N distributed components (stochastic processes) is $C = 3N - 1$.

This Gaussian Mixture Model based clustering with Bayesian Information Criterion is used to find the most stable distribution of the mixture components in the brain volume. Fig. 1 shows a BIC value plot for real fMRI data obtained from a single subject. Here, when the algorithm achieves the minimum BIC value for four clusters and does not reduce further, then according to BIC these four clusters are the optimal clusters for this subject's data.

3. Materials and methods

3.1. Artificial fMRI dataset

The artificial dataset has been generated using the boxcar sequence of various frequencies correlated with different cubical

Table 1
Characteristic details of AD subjects.

Patient	Sex	Age
1	F	75
2	M	87
3	F	63
4	F	72
5	F	63
6	M	87

blocks as placed in the brain phantom/mask (Dimitriadou et al., 2004). We generated six artificial datasets with different Signal-to-Noise Ratios SNRs (Dimitriadou et al., 2004) (for SNR values 16, 8, 4, 2, 1 and 0 dB) contaminated with additive white Gaussian noise (AWGN) (MATLAB, 2012; Chen and Tyler, 2008). Also, six datasets with added Rician noise (RN) (Sled et al., 1998) for SNR values of 16, 14, 12, 10, 8, and 6 dBs were also created. Rician noise was generated using the "Rice/Rician distribution" toolbox (RDT) for MATLAB. These datasets have been formed using activation blocks of variable frequency ranging from 0.01 Hz to 0.08 Hz (Chen and Tyler, 2008; Raichle et al., 2001; Yang et al., 2007).

A standard brain phantom/mask of volume $61 \times 73 \times 61$ voxels was employed. Eighteen blocks of volume $12 \times 12 \times 12$ each were formed. The scans were then modulated with different frequencies to generate the activations corresponding to those frequencies of low speed fluctuations between 0.01 Hz and 0.08 Hz across 140 scans. These noiseless 3D brain volumes were contaminated with the aforementioned noise signals. We have used the available MATLAB function for generating AWGN for different SNRs. Similarly for Rician noise, the initial steps were the same for the noiseless data preparation then Rician type noise was added for different SNRs. For the Rician noise function (Sled et al., 1998) it was not possible to define the precise value of SNRs, and it was not possible to produce SNR values less than 6 dB approx. Therefore, we generated various combinations of s and v values as given below:

$$R \sim ricernd(v,\ s),$$

where $R = \sqrt{X^2 + Y^2}$, $X \sim N(v\cos(a), s^2)$ and $Y \sim N(v\sin(a), s^2)$. These combinations of s and v were tested for dB SNR using the mean (μ) and standard deviation (σ) (as shown below in (6)) calculated using the *ricestat* function as given in the Rice/Rician Distribution Toolbox (RDT) for MATLAB developed in 2008 by G. Ridgway http://www.mathworks.com/matlabcentral/fx_files/14237/3/rician.zip (Sled et al., 1998).

$$dB_{\mathrm{SNR\_Rician}} = 20\log_{10}\left(\frac{\mu}{\sigma}\right) \tag{6}$$

3.2. Real fMRI datasets

The fMRI dataset from the ADNI online data repository was recorded from a total of 6 (4 females and 2 males) AD patients, where all the subjects were aged 60 years or older. All subjects were instructed to remain in the resting state but awake and not to think anything specific during the data acquisition. These scans were acquired using a Philips Medical Systems Integra 3T scanner, where the time of repetition (TR) and time of echo (TE) were 3000 ms and 30 ms, respectively. A total of 140 (420 s) whole-brain ($64 \times 64 \times 48$) scans were recorded for each subject; here the thickness of each voxel was 3.3 mm. Further details are given in Table 1.

3.3. Proposed method

The first step was to pre-process the available artificial and real datasets. The SPM toolbox (Friston et al., 1994; MATLAB, 2012) was used for pre-processing the data. All the pre-processing steps were very similar to the previous study (Garg et al., 2011a) except the normalization, where we developed a template for one subject using the available Montreal Neurological Institute (MNI) template and then normalized the other subjects to that template (Song et al., 2011). This step is required to make the headshape comparable among the subjects and to analyse them together for similar types of activation patterns in resting state data (Raichle et al., 2001). The other steps included re-slicing and re-aligning, co-registering, segmentation and smoothing (Ashburner et al., 2012). De-trending of the time-series data for all the voxels was also performed to remove any linear trends and to minimize the effects of the changes in the data characteristic due to thermal effects and various other equipment related constraints (Song et al., 2011).

3.3.1. The ALFF method

After the preparation of the datasets, the data were spatially smoothed and low pass filtered below 0.01 Hz, as the DMN has been found to be consistent up to this frequency; also respiration and pulse artefacts are much less prominent up to this frequency (Raichle et al., 2001). A frequency power spectrum analysis of the time-series was observed at each voxel. The power spectrum was calculated by squaring the amplitude in frequency domain using the fast Fourier transform (FFT).The averaged square root of the power spectrum was performed to calculate the average amplitude of activation for the required range of 0.01–0.08 Hz. This averaged square root is referred to as Amplitude of Low-Frequency Fluctuation (ALFF) (Yang et al., 2007; Song et al., 2011). ALFF has been scaled by the global mean value for the regions corresponding to a mask obtained for the brain structure.

3.3.2. The GMM-ALFF method

After pre-processing of the given fMRI data, GMM was applied on the data to reduce the effect of noise by distributing the data in an optimal number of clusters, selected using the Bayesian Information Criterion (BIC) (Fonseca, 2008). These steps were repeated one-by-one for each subject (cf. Fig. 2 for an illustration of the steps). Subsequently, the data were processed using the same approach to that applied for the ALFF method (Yang et al., 2007; Song et al., 2011) described in the previous section.

4. Results

Many of the clustering performance calculation methods have used the Jaccard's coefficient (Dimitriadou et al., 2004) as an index of measurement and validation of the calculated results with respect to the known reference template, where the regions of true activity are already known. In this work the aim is to use a method that is capable of finding the true activations and at the same time not misidentifying the regions of activation. A modified coefficient of accuracy $J_{accuracy}$ is therefore calculated as the ratio of the sum of true positives (TPs) and True Negatives (TNs) and the sum of true positives (TPs), false positives (FPs), True Negatives (TNs) and false negatives (FNs) (Demirci et al., 2008).

$$J_{accuracy} = \frac{TPs + TNs}{TPs + FPs + TNs + FNs} \tag{7}$$

The reliability and robustness of the proposed algorithm has been estimated for those cases where the variation between active and inactive regions is minimal and thus identification of boundaries between individual regions is difficult. For this we considered the precision index calculation $J_{precision}$. The precision index provides information about the performance of an algorithm that can

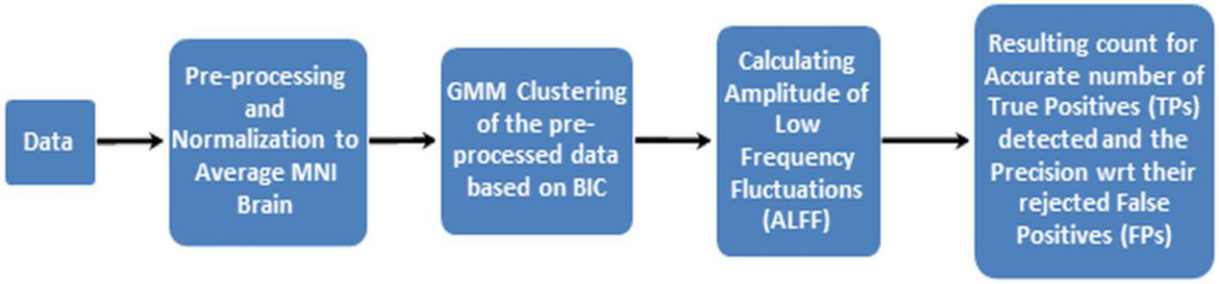

Fig. 2. Calculation steps of the proposed ALFF with GMM algorithm.

Table 2
Comparison between ALFF and GMM-ALFF methods for artificial AWGN data.

SNR (dB)	ALFF Without GMM (%)		ALFF with GMM (%)		Wilcoxon signed-rank test *p*-value	
	Accuracy	Precision	Accuracy	Precision	Accuracy	Precision
16	100	99	100	100	0.0625	0.0313
8	94	51	100	100		
4	87	32	100	97		
2	83	26	100	96		
1	81	25	99	87		
0	80	23	97	65		

ideally avoid False Positives (FPs) and the algorithm's precision in detecting regions which are truly active (Dettori and Semler, 2007).

$$J_{precision} = \frac{TPs}{TPs + FPs} \quad (8)$$

4.1. Artificial data (with AWGN noise)

4.1.1. ALFF method

Table 2 presents a comparison of the accuracy and precision results between the ALFF and GMM-ALFF methods for artificial data with different levels of AWGN. As can be seen from the results (cf. Table 2), the precision of the ALFF method is lower than GMM-ALFF for SNR less than 16 dB, while it is capable of characterizing the true positives for even 1 dB SNR but at the same time it appears unreliable because of the detection of false regions of activation as shown (cf. Fig. 3(a) and (b)). It can be clearly seen from the images given in Fig. 3(b) that the effect of noise is apparent on the ALFF for even 8 dB SNR case whilst for GMM-ALFF the activation detection is consistent even at highest levels of noise.

4.1.2. GMM-ALFF method

In comparison to the ALFF method, it can be seen from the results (cf. Table 2) that the precision of GMM-ALFF reduces severely only for the SNR less than 4 dB (cf. Fig. 3(c) and (d)). The images given in Fig. 3(d) clearly show that the GMM-ALFF approach is only affected with noise significantly below 2 dB noise cases. Table 2 shows that the differences in the accuracy and precision values obtained by two approaches are more than 15% and 40%, respectively. When tested with Wilcoxon signrank test these difference between the methods (cf. Table 2) were found to be statistically significant ($p < 0.05$) in terms of precision ($p = 0.0313$), but the difference in terms of accuracy ($p = 0.0625$) are not.

4.2. Artificial data (with Rician noise)

4.2.1. ALFF method

The data with added Rician noise was processed in the same way as that with AWGN. The slices in Fig. 4(b) show that patches of noise are clearly visible for low SNR of 8 dB and 6 dB. The effect of Rician noise was not as severe as the AWGN, as can be seen from the images (cf. Fig. 4(b) and (d) and also from Table 3). The traditional ALFF method worked quite well in identifying the regions of activations, but the GMM-ALFF significantly outperformed the traditional ALFF for precision in avoiding false activations, as discussed next.

4.2.2. GMM-ALFF method

The GMM based method generated better results for the Rician noise. From Fig. 4(c) and (d), we can clearly see that noise levels up to 8 dB are not substantial but been suppressed effectively and visually there is minimal evidence noise, which has been further verified with the statistical analysis. In fact, the accuracy and precision remained constant at 100% for various noise cases whereas the classic ALFF method resulted in gradual reduction in accuracy as well as precision with the decreasing SNR (cf. Table 3). The improvement in the precision values obtained was up to 25% for the 6 dB SNR. For the Rician noise case the results suggest the improvement in accuracy and precision given by the GMM based approach are significant: Accuracy ($p = 0.05$) and precision ($p = 0.031$).

4.3. Real data mixed with AWGN

For evaluating the noise reducing capability of GMM, we also injected the same levels of noise in the real data as we did for the artificial datasets as discussed below.

4.3.1. ALFF method

The fMRI slices displayed in Fig. 5(a) and (b) are from subject 1 out of the 6 subjects, where data was contaminated with AWGN for SNRs values of 16, 8, 4, 2, 1 and 0 dB, respectively, from left to right. As can be seen from Fig. 5(a) and (b), when the ALFF was applied on the data with 1 dB SNR, it got distorted so heavily that the ALFF without GMM could not even recover the whole slice.

4.3.2. GMM-ALFF method

As can be seen from the slices in Fig. 5(c) and (d), the proposed GMM based ALFF method successfully recovered the whole slice for all SNR values. It achieved higher cross-subject mean accuracy and precision (cf. Table 4) than the ALFF without GMM approach. Below the SNR value of 16 dB (cf. Table 4) the differences between ALFF with and without GMM were significant ($p < 0.05$) (a Wilcoxon signed rank statistical test was applied on the 6 data-sets from all six subjects). The precision of the observed activation regions for the fMRI data was more than 4% higher on average when GMM is

Table 3
Comparison between ALFF and GMM-ALFF methods for artificial RN data.

SNR (dB)	ALFF Without GMM (%)		ALFF with GMM (%)		Wilcoxon signed-rank test *p*-value	
	Accuracy	Precision	Accuracy	Precision	Accuracy	Precision
16	100	99	100	100	0.050	0.0313
14	100	99	100	100		
12	100	99	100	100		
10	100	99	100	100		
8	99	98	100	100		
6	97	75	100	100		

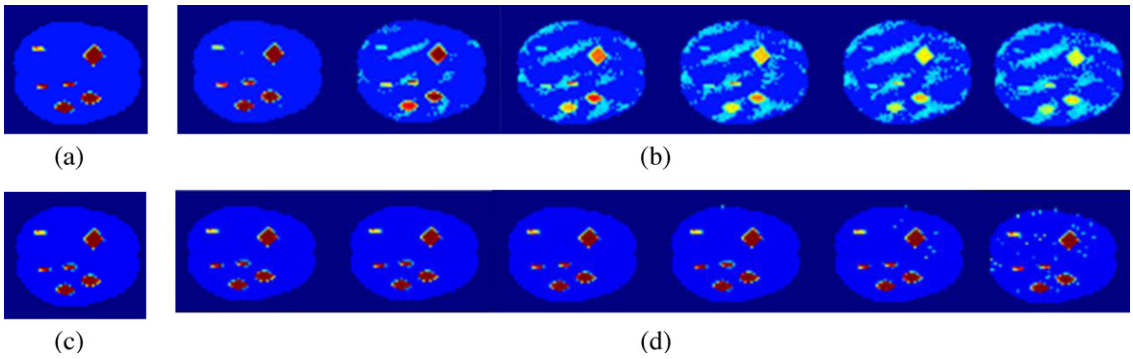

Fig. 3. Brain fMRI slice for artificial data with AWGN: with ALFF alone (a) reference template and (b) results; and similarly, for ALFF with GMM: (c) reference template, and (d) results for SNR of 16, 8, 4, 2, 1 and 0 dB, respectively, from left to right.

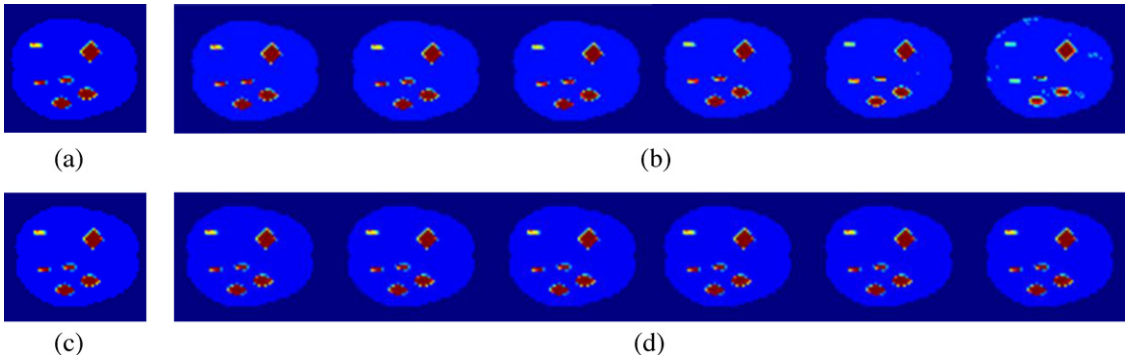

Fig. 4. Brain fMRI slice for artificial data with RN: for ALFF alone (a) reference template and (b) results; and similarly, for ALFF with GMM: (c) reference template and (d) results for SNR of 16, 14, 12, 10, 8 and 6 dB respectively from left to right.

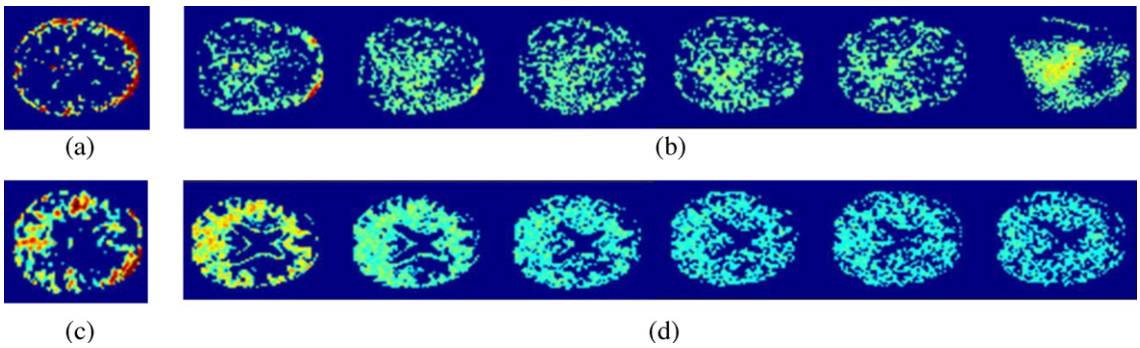

Fig. 5. Brain fMRI slice for sub 1 data with AWGN: for ALFF alone (a) reference template and (b) results; and similarly for ALFF with GMM: (c) reference template and (d) results for SNR of 16, 8, 4, 2, 1 and 0 dB respectively from left to right.

Table 4
Comparison between ALFF and GMM-ALFF methods for real AWGN data for 6 subjects.

SNR (dB)	ALFF (mean) (%)		ALFF with GMM (mean) (%)		Wilcoxon signed-rank test *p*-value	
	Accuracy	Precision	Accuracy	Precision	Accuracy	Precision
16	70	59	73	64	0.09375	0.03125
8	68	57	72	61	0.03125	0.03125
4	68	56	70	60	0.03125	0.03125
2	68	56	70	59	0.03125	0.03125
1	66	57	69	59	0.0625	0.03125
0	64	56	69	59	0.0625	0.03125

Table 5
Comparison between ALFF and GMM-ALFF methods for real data with RN for six subjects.

SNR (dB)	ALFF (mean) (%)		ALFF with GMM (mean) (%)		Wilcoxon signed-rank test *p*-value	
	Accuracy	Precision	Accuracy	Precision	Accuracy	Precision
16–6	84	80	86	83	0.03125	0.03125

used, which is a substantial improvement over the ALFF without GMM based method.

4.4. Real data mixed with Rician noise

Adding Rician noise in real data provided similar results to those obtained for the artificial data. The procedure to apply the Rician noise was similar to the artificial data. We observed the effect of applying our proposed GMM-ALFF method in comparison to the classical ALFF approach. Both methods were able to maintain the consistency for noise removal for various SNR levels, although GMM based ALFF again outperformed the traditional ALFF method significantly for both accuracy and precision ($p < 0.05$) (cf. Table 5 and Fig. 6). The improvement in the mean precision across 6 subjects was at least 3% for all the noise cases which suggests that GMM-ALFF would provide less false activations than a traditional ALFF. Again the differences are statistically significant.

The results thus show that the GMM based approach can improve the accuracy in both the artificial and real data cases with varying noise levels of different types, Gaussian and Rician. The other significant improvement was not only the consistency of better results for low SNR values of up to 4 dB in cases of Gaussian Noise and 6 dB in case of Rician Noise, but also preserving all fMRI brain regions by being robust to higher noise values in cistern areas, where the classic ALFF (cf. Figs. 5(b) and 6(b)) method has failed severely.

5. Discussion

This study mainly investigated the effects of noise on the processing of fMRI images. It has been suggested in the literature that when the objective is to analyse disease related changes, analysing resting state data is more meaningful because of the differences in the ways of performing a specific action by various subjects (Raichle et al., 2001; Yang et al., 2007). For example, it is much easier for the operator and much less onerous on the participant, particularly if they suffer from conditions such as AD, to ask the participant to relax as opposed to performing a task which involves memory challenges and movement to react to stimuli. This can be daunting for participants. There are several methods suggested to analyse BOLD resting state data obtained from fMRI where calculating the low frequency responses from the fMRI data has been suggested as the most suitable due to fact that the higher frequency responses are affected by noise more. The REST toolbox (Song et al., 2011) for resting state fMRI has included a method for low frequency response analysis, the Amplitude of Low Frequency Fluctuation (ALFF) (Yang et al., 2007) tested in this work, which can be used to calculate the low frequency changes in the fMRI data as described previously. This toolbox performs well under low noise conditions. But the high noise in the fMRI environment especially near to the cistern areas can obscure the underlying BOLD processes. To account for this, we have developed a GMM based method to perform a noise stabilizing step before the ALFF analysis. In this paper, our method has been applied for processing an artificial data-set as well as an Alzheimer's Disease patients' datasets and has resulted in significant performance improvements. The artificial data-set was injected with additive white Gaussian noise (AWGN) for creating data with six different SNR values. The AWGN applied artificial datasets were recovered well for up to 2 dB SNR when GMM-ALFF was applied, while for ALFF without GMM, the precision reduced by 48% approx. below 16 dB SNR. Similarly, datasets with added Rician noise (RN) were also recovered well for

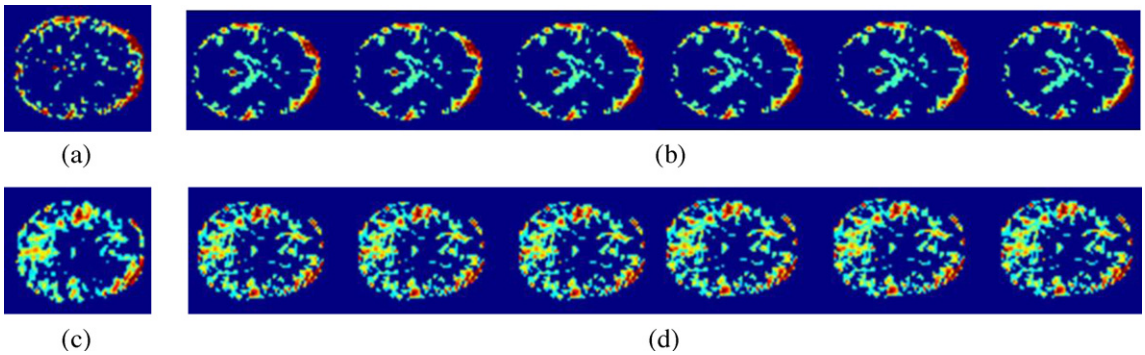

Fig. 6. Brain fMRI slice for sub 1 real data with RN: for ALFF alone (a) reference template and (b) results; and similarly, for ALFF with GMM: (c) reference template and (d) results for SNR of 16, 14, 12, 10, 8 and 6 dB respectively from left to right.

all the noise cases though with statistically significant differences for 6 dB SNR only. Along with the average improvement of 4% in precision values for real data with AWGN, our GMM based approach was able to recover whole brain structure (cf. Fig. 5(d)) where classic ALFF failed for SNR less than 4 dB (cf. Fig. 5(b)). This suggests that the ALFF method is more prone to information loss due to the noise generated in the fMRI environment. An important aspect worth highlighting in terms of the activation detection provided by the ALFF alone is that the regions of activation mainly near to the cistern areas were affected heavily by fMRI environmental noise, while the GMM based method was able to recover the activity in whole brain including cistern areas. This is also depicted in the consistency of the changes in the activation pattern for the increasing noise cases where ALFF provided significant changes from cistern regions to whole slice while GMM based ALFF showed more stability in the resulting patterns for increasing noise. The percentage improvement in the case of RN applied on real data is also 3% on average with the similar improvement in noise stabilization for cistern regions as found in the AWGN cases. Unlike artificial data, percentage improvement for real data is stated very less, because for real data we do not have a noiseless template to refer, therefore we have only stated the relative stability of proposed algorithm for additional Gaussian and Rician noise to already noisy reference brain data.

Although the GMM method was found to make significant improvement in performance, there are a few limitations in using this method, which are mainly related to the computational resource and time required. Being an expectation maximization based algorithm, this method requires load all the data arrays in memory and to find the true global optima for the whole data and therefore requires substantial memory. Also, decision about the number of clusters is made based on a minimum BIC value obtained after exhaustively searching various cluster combinations. This needs several iterations to calculate the three characteristic parameters: mean, standard deviation and proportion of the data. The time taken by this calculation increases exponentially with the number of possible clusters.

Overall, the advantages for noise stability in precision values over computational time and resources are more important as the data is being processed offline and suggests that GMM can provide significant improvement when used together with the ALFF method.

6. Conclusion and future work

A method to reduce the noise effects from the resting state fMRI data of AD patients has been proposed. The results suggest that treating the data with GMM before performing the activation detection and analysis using the ALFF method for resting state data significantly improves the results. This GMM-ALFF approach has been compared with the existing ALFF method for the analysis of artificial as well as real resting state fMRI data. For the AWGN, the GMM supported ALFF was found stable for the SNR level as low as 2 dB, while the ALFF alone failed below the noise levels of 16 dB SNRs. Similarly for the RN mixed data, an improvement of more than 40% was recorded in precision with GMM based ALFF. Also, we applied these methods on real data with the same AWGN and RN and found significant differences in the results of more than 3% for precision (or rate of generation of false positives) given by the proposed GMM-ALFF method. GMM based clustering is stable and the results are reproducible, therefore it can be successfully used where other clustering methods suffer some uncertainty in the resulting number of clusters. Here, we have successfully incorporated BIC to decide the optimum number of clusters. The future work already underway is to develop a stand-alone method to find the regions of activation for the underlying default mode processes in the resting state data including analysis of changes in the BOLD based on the movement of the clusters. This variability of clusters would provide information about the spontaneity of the changes in various brain regions. Another method based on BOLD correlations with low frequency changes in fMRI, which is based on our previous research (Garg et al., 2011a) for activation region detection in a specific paradigm based data using GMM is also being developed.

Acknowledgements

Mr. Gaurav Garg is supported by the Computational Neuroscience Research Team under the N. Ireland Department for Education and Learning – “Strengthening the All-island Research Base” project.

Data used in the preparation of this article were obtained from the Alzheimer’s Disease Neuroimaging Initiative (ADNI) database (adni.loni.ucla.edu). The ADNI was launched in 2003 by the National Institute on Aging (NIA), the National Institute of Biomedical Imaging and Bioengineering (NIBIB), the Food and Drug Administration (FDA), private pharmaceutical companies and non-profit organizations, as a $60 million, 5-year public private partnership.

References

Ashburner J, Chen C, Moran R, Henson R, Glauche V, Phillips C. SPM8 Manual. London, UK: Functional Imaging Laboratory, Wellcome Trust Centre for Neuroimaging, Institute of Neurology, UCL; 2012. p. 475.

Buxton RB, Wong EC, Frank LR. Dynamics of blood flow and oxygenation changes during brain activation: the balloon model. Magn Reson Med 2005;39:855–64.

Chen C, Tyler CW. Spectral analysis of fMRI signal and noise. In: Onozuka M, Yen C, editors. Novel trends in brain science. Japan: Springer; 2008. p. 63–76.

Demirci O, Clark VP, Magnotta VA, Andreasen NC, Lauriello J, Kiehl KA, Pearlson GD, Calhoun VD. A review of challenges in the use of fMRI for disease classification/characterization and a projection pursuit application from a multi-site fMRI schizophrenia study. Brain Imaging Behav 2008;2:207–26.

Dettori L, Semler L. A comparison of wavelet, ridgelet, and curvelet-based texture classification algorithms in computed tomography. Comput Biol Med 2007;37:486–98.

Dimitriadou E, Barth M, Windischberger C, Hornik K, Moser E. A quantitative comparison of functional MRI cluster analysis. Artif Intell Med 2004;31:57–71.

Fonseca JRS. The application of mixture modeling and information criteria for discovering patterns of coronary heart disease. J Appl Quan Meth 2008;3:292–303.

Friston KJ, Holmes AP, Worsley KJ, Poline JP, Frith CD, Frackowiak RSJ. Statistical parametric maps in functional imaging: a general linear approach. Hum Brain Mapp 1994;2:189–210.

Garg G, Prasad G, Garg L, Coyle D. Gaussian mixture models for brain activation detection from fMRI data. Int J Bioelectromagn 2011a;13:255–60.

Garg L, McClean S, Meenan B, Millard P. Phase-type survival trees and mixed distribution survival trees for clustering patients’ hospital length of stay. Informatica 2011b;22:57–72.

Garg L, McClean S, Meenan B, El-Darzi E, Millard P. Clustering patient length of stay using mixtures of Gaussian models and phase type distributions. In: Proceedings of the IEEE International Symposium on Computer-Based Medical Systems; 2009. p. 1–7.

Keller CJ, Bickel S, Entz L, Ulbert I, Milham MP, Kelly C, Mehta AD. Intrinsic functional architecture predicts electrically evoked responses in the human brain. Proc Natl Acad Sci 2011;108:10308–13.

MATLAB® The MathWorks Inc.: Natick, MA, 2012.

Raichle ME, MacLeod AM, Snyder AZ, Powers WJ, Gusnard DA, Shulman GL. A default mode of brain function. Proc Natl Acad Sci 2001;98:676–82.

Sled JG, Zijdenbos AP, Evans AC. A nonparametric method for automatic correction of intensity nonuniformity in MRI data. IEEE T Med Imaging 1998;17:87–97.

Song XW, Dong ZY, Long XY, Li SF, Zuo XN, Zhu CZ, He Y, Yan CG, Zang YF. REST: a toolkit for resting-state functional magnetic resonance imaging data processing. PLoS ONE 2011;6:e25031.

Weiner MW, Veitch DP, Aisen PS, Beckett LA, Cairns NJ, Green RC, Harvey D, Jack CR, Jagust W, Liu E. The Alzheimer’s disease neuroimaging initiative: a review of papers published since its inception. Alzheimers Dement 2012;8:S1–68.

Yang H, Long XY, Yang Y, Yan H, Zhu CZ, Zhou XP, Zang YF, Gong QY. Amplitude of low frequency fluctuation within visual areas revealed by resting-state functional MRI. Neuroimage 2007;36:144–52.